IEEE Access
Multidisciplinary ⋮ Rapid Review ⋮ Open Access Journal

Received October 13, 2016, accepted November 29, 2016, date of publication January 20, 2017, date of current version March 15, 2017.

Digital Object Identifier 10.1109/ACCESS.2016.2640559

Reconstruction of Angular Kinematics From Wrist-Worn Inertial Sensor Data for Smart Home Healthcare

EMMA VILLENEUVE[1], WILLIAM HARWIN[2], WILLIAM HOLDERBAUM[2,3], BALAZS JANKO[2], AND R. SIMON SHERRATT[2], (Fellow, IEEE)

[1]National Institute for Health Research, Collaboration for Leadership in Applied Research and Care in South West Peninsula, University of Exeter, Exeter EX1 2LU, U.K.
[2]Department of Biomedical Engineering, University of Reading, Reading RG6 6AY, U.K.
[3]Faculty of Science and Engineering, Manchester Metropolitan University, Manchester M1 5GD, U.K.

Corresponding author: E. Villeneuve (e.villeneuve@exeter.ac.uk)

This work was supported by the U.K. Engineering and Physical Sciences Research Council through SPHERE IRC under Grant EP/K031910/1.

ABSTRACT This paper tackles the problem of the estimation of simplified human limb kinematics for home health care. Angular kinematics are widely used for gait analysis, for rehabilitation, and more generally for activity recognition. Residential monitoring requires particular sensor constraints to enable long-term user compliance. The proposed strategy is based on measurements from two low-power accelerometers placed only on the forearm, which makes it an ill-posed problem. The system is considered in a Bayesian framework, with a linear-Gaussian transition model with hard boundaries and a nonlinear-Gaussian observation model. The state vector and the associated covariance are estimated by a post-regularized particle filter (constrained-extended-RPF or C-ERPF), with an importance function whose moments are computed via an extended Kalman filter (EKF) linearization. Several sensor configurations are compared in terms of estimation performance, as well as power consumption and user acceptance. The proposed constrained-EKF (CERPF) is compared to other methods (EKF, constrained-EKF, and ERPF without transition constraints) on the basis of simulations and experimental measurements with motion capture reference. The proposed C-ERPF method coupled with two accelerometers on the wrist provides promising results with 19% error in average on both angles, compared with the motion capture reference, 10% on velocities and 7% on accelerations. This comparison highlights that arm kinematics can be estimated from only two accelerometers on the wrist. Such a system is a crucial step toward enabling machine monitoring of users health and activity on a daily basis.

INDEX TERMS Accelerometer, kinematics, joint angle, ill-posed problem, particle filter, extended Kalman filter, constraint.

I. INTRODUCTION

Orientation is a key motivation for the use of inertial sensors. Indeed, Micro Electro Mechanical System (MEMS) accelerometers and more generally Inertial Measurement Units (IMU) are often referred as tilt sensors. Historically, IMUs, which are constituted of a 3D accelerometer, a 3D gyroscope and optionally a magnetometer, are commonly used as navigation systems for aircraft. They provide the orientation and motion of the moving body. The use of inertial sensors has now widely spread to the biomedical community [1], [2], combining sometimes inertial and physiological sensors [3]. This interest is partly due to the very low price and the compactness of IMU sensors. Moreover, they are accessible to the general public inside smartphones, smart watches and fitness bands.

Inertial sensors, in particular accelerometers, have grown in importance both to quantify human performance and to identify human activity. Human performance quantification is usually concerned with the estimation of the joint angle of the limbs [4], in particular for gait analysis [5]–[9] where sensors can be embedded into pockets attached to individual limbs. Activity estimation has now developed to the point where several commercial wrist worn devices are now available to give feedback to the individual on their daily performance.

2169-3536 © 2017 IEEE. Translations and content mining are permitted for academic research only.
Personal use is also permitted, but republication/redistribution requires IEEE permission.
See http://www.ieee.org/publications_standards/publications/rights/index.html for more information.

While gait analysis is commonly based on lower limb joint angles (e.g. [10]–[13]), it is interesting to notice that it can also benefit from angular velocities [14]. So, joint angles and kinematics are useful features for activity classification, combined with acceleration intensity such as in [15], or with depth camera in [2]. Upper limbs are also studied, focussing on shoulder and elbow joint [16], for instance for tremor estimation [17]. Similarly, the inertial sensors are placed on robot arms to check their positions, as for brachytherapy [18]. The difficulty addressed in this paper is to allow a minimal set of worn sensors to both reconstruct information such as joint angles and to allow this information to be integrated into a wider context of activity recognition where other information may be able to refine the accuracy of the judgement.

The work presented in this paper is part of the EPSRC funded SPHERE project which is collecting data from a wide range of sensors that can quantify activity in a residential environment, including sensors worn by the occupants, in-order to quantify, analyse and feedback information relating to health and healthcare. The SPHERE concept is to provide a generic tool to describe the living behaviours of people in a residential environment that can encode health related information. Although this could include critical events such as medical emergencies, the data on long term activities and behaviours that are markers of health provides the more specific focus. SPHERE will be mainly used by residents, but also by their family, carers and medical staff. The initial suite of sensors that will be deployed into up to 100 homes in the Bristol area of the UK will include a number of wearable sensors providing inertial data, environment sensors and data processed video streams that anonymize the individual [19]. It is anticipated that some of the conditions that would be observed in this study will include individuals with COPD (chronic obstructive pulmonary disease), Parkinson's disease, cognitive difficulties including Alzheimer's, orthopaedics difficulties, and nonspecific problems relating to frailty.

This paper aims at providing an estimation the angle, angular velocity and acceleration of human limbs and the associated standard deviations, from accelerometers on the second segment such as the forearm or the shank. The method could be implemented on the central coordinating node of the sensor network, as proposed in [20]. In the data processing chain, this method is an analysis step that provides advanced features, useful to evaluate the quality of movement. The estimated kinematic variables can also be used as basis for statistical features, as a complement to other sensing modalities such as depth cameras [2], [21], for activity classification. In long-term residential monitoring, these kinematic variables can build an individualized pattern of activities and help to detect an abnormal situation. A key point in this research is the fact that the sensors data based estimation has several solutions which makes it an ill-posed problem. This paper focuses on the different ways to solve this inverse problem, such as the use of prior information containing biomechanical constraints. In particular, the estimation problem is tackled in a Bayesian framework, approximating the posterior distribution by a Regularized Particle Filter.

Section II describes the kinematic model of a 2-link chain, as well as transition and observation models of data. Section III presents existing, proposed estimation methods and relevant criteria for residential monitoring. Then, the performances of the proposed method are examined, in comparison with other sensor configurations and other estimation methods, from a simulated dataset (section IV) and an experimental dataset (section V).

II. PROBLEM STATEMENT

As we will, in the proposed methods, take into account a parametric model for the kinematics of the human body, we describe in this section, the kinematics of a 2-link chain that simply models an arm or a leg. For sake of simplicity, the kinematics are studied in a single plane, typically the sagittal plane that contains the major part of arm and leg motions. Moreover, the evolution of the kinematics variables and their measurement are statistically represented through transition and observation models.

A. KINEMATIC MODEL OF A 2-LINK PLANAR CHAIN

The aim of this study is to estimate the angle ϕ, angular velocity ω and angular acceleration α of both segments of a 2-link planar chain. The unknown kinematic variables are gathered in the following vector:

$$\boldsymbol{x}^{(i)} = [\phi_i, \omega_i, \alpha_i]^T \tag{1}$$

where $i \in \{1, 2\}$ is the link number. The state vector gathers the kinematics of both links:

$$\boldsymbol{x} = \left[\boldsymbol{x}^{(1)T}, \boldsymbol{x}^{(2)T}\right]^T \tag{2}$$

As can be seen in Fig. 1, the first angle corresponds to the rotation between the reference system of coordinates $(O, \boldsymbol{x}_0, \boldsymbol{y}_0)$ and the first local system $(O, \boldsymbol{x}_1, \boldsymbol{y}_1)$, the second angle is the rotation between the first system and the second $(O_2, \boldsymbol{x}_2, \boldsymbol{y}_2)$. Note that all angles are defined in the interval $]-\pi; \pi]$.

In this study, the estimation of kinematics is based on measurements from accelerometers. These measurements depend on the motion of the link and the placement of the sensor. The absolute acceleration of a point located on the first link, written in the local system $(O, \boldsymbol{x}_1, \boldsymbol{y}_1)$, is given by the mechanical model:

$$h^{(1)}(\boldsymbol{x}_t^{(1)}, \ell_1) = \begin{pmatrix} -\ell_1\omega_{1,t}^2 - g\cos\phi_{1,t} \\ \ell_1\alpha_{1,t} + g\sin\phi_{1,t} \end{pmatrix} \tag{3}$$

where ℓ_1 is the distance of the point from the origin of the link, t is the time index, g is the norm of the gravitational vector. Note that the origin of the pendulum is assumed static.

Moreover, the acceleration of a point located on the second link, written the local system $(O, \boldsymbol{x}_2, \boldsymbol{y}_2)$, is given by the

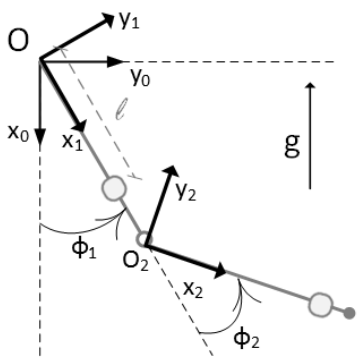

FIGURE 1. Two-link planar chain. The reference coordinate system is (O, x_0, y_0). The system (O, x_1, y_1) (resp. (O_2, x_2, y_2)) is attached to the first link (resp. second link). The vector g is the gravitational acceleration.

following function $h^{(2)}$:

$$h^{(2)}(\boldsymbol{x}_t, L, \ell_2) = h^{joint}(\boldsymbol{x}_t, L) + h^{(1)}(\boldsymbol{x}_t^{(1)} + \boldsymbol{x}_t^{(2)}, \ell_2) \quad (4)$$

where L is the length of the first link, ℓ_2 is the distance of the point from the local origin O_2, $h^{(1)}$ is evaluated at the sum vector $\boldsymbol{x}_t^{(1)} + \boldsymbol{x}_t^{(2)}$ instead of $\boldsymbol{x}_t^{(1)}$ and h^{joint} is the acceleration of the joint, in the same system $(O, \boldsymbol{x}_2, \boldsymbol{y}_2)$:

$$h^{joint}(\boldsymbol{x}_t, L) = \begin{pmatrix} -L\omega_{1,t}^2 \cos(\phi_{2,t}) + L\alpha_{1,t} \sin(\phi_{2,t}) \\ L\omega_{1,t}^2 \sin(\phi_{2,t}) + L\alpha_{1,t} \cos(\phi_{2,t}) \end{pmatrix} \quad (5)$$

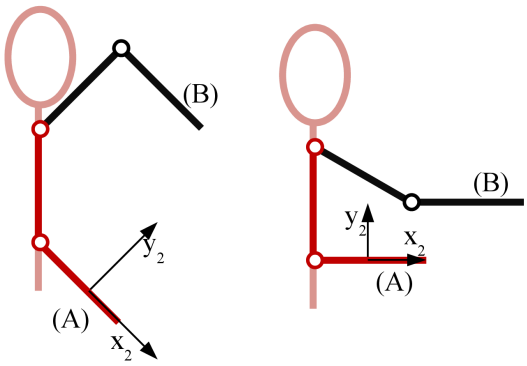

FIGURE 2. Example of two arm static configurations leading to the same observation. Left: $x_A = \left[0, 0, 0, \frac{\pi}{4}, 0, 0\right]$ $x_B = \left[\frac{3\pi}{4}, 0, 0, -\frac{\pi}{2}, 0, 0\right]$. Right: $x_A = \left[0, 0, 0, \frac{\pi}{2}, 0, 0\right]$ $x_B = \left[\frac{\pi}{3}, 0, 0, \frac{\pi}{6}, 0, 0\right]$. In both cases, $h^{(2)}(x_A, L, \ell_2) = h^{(2)}(x_B, L, \ell_2)$.

B. OBSERVABILITY

The system is observable if the state vector can be fully determined from a noise-free set of observations. Fig. 2 shows that two configurations of the arm lead to the same position and motion of sensors on the wrist. As a consequence, estimating the state from the observation only will equally drive to one of these solutions. For mathematical consideration of the observability of this problem, one can refer to [22]. On the left part of Fig. 2, the black configuration is unrealistic because of the hard constraint of the elbow: ϕ_2 should remain, for most people, positive. On the right part, both configurations are humanly possible.

As several configurations can provide the same observations, then estimating this state vector is an ill-posed problem. To solve it, it is essential to bring some additional information of smoothness and constraint through the transition distribution.

C. STATISTICAL TRANSITION MODEL

The transition model describes the probability distribution of the kinematic vector $\boldsymbol{x}_t$ at time t as a function of the former value $\boldsymbol{x}_{t-1}$. A linear transition model is sufficient to capture a joint movement and it allows to reduce computation cost [22]. For the kinematics of one link, the statistical transition model combines a linear evolution and a perturbation noise:

$$\boldsymbol{x}_t^{(i)} = F^{(1)}\boldsymbol{x}_{t-1}^{(i)} + \boldsymbol{v}_t \quad \text{with } \boldsymbol{v}_t \sim \mathcal{N}(\boldsymbol{0}, Q^{(i)}) \quad (6)$$

where $F^{(1)} \in \mathbb{R}^{3\times3}$ is the linear transition matrix for one link and $\mathcal{N}(\boldsymbol{0}, Q^{(i)})$ a centred Gaussian noise of covariance matrix $Q^{(i)} \in \mathbb{R}^{3\times3}$ for the variables for the ith link. As the result of the Taylor series approximation, the transition matrix for one link [22] is given by the following expression:

$$F^{(1)} = \begin{pmatrix} 1 & \Delta T & \frac{\Delta T^2}{2} \\ 0 & 1 & \Delta T \\ 0 & 0 & 1 \end{pmatrix} \quad (7)$$

where ΔT is the sampling period, or more generally the time interval between the two samples $\boldsymbol{x}_{t-1}^{(i)}$ and $\boldsymbol{x}_t^{(i)}$.

This study estimates the angular kinematics of both links at the same time. The transition is derived from the former transition equation as follows:

$$\boldsymbol{x}_t = F\boldsymbol{x}_{t-1} + \boldsymbol{v}_t \quad (8)$$

where F is the transition matrix for two links:

$$F = \begin{pmatrix} F^{(1)} & \boldsymbol{0}_3 \\ \boldsymbol{0}_3 & F^{(1)} \end{pmatrix} \text{ with null matrix } \boldsymbol{0}_3 \in \mathbb{R}^{3\times3},$$

and $\boldsymbol{v}_t$ is the transition perturbation for two links:

$$\boldsymbol{v}_t \sim \mathcal{N}(\boldsymbol{0}, Q) \text{ with } Q = \begin{pmatrix} Q^{(1)} & \boldsymbol{0}_3 \\ \boldsymbol{0}_3 & Q^{(2)} \end{pmatrix}.$$

In this study, the estimation is clearly an ill-posed inverse problem, so we need to introduce as much information as possible to find a meaningful solution. In addition to the linear model which is commonly used, biomechanical constraints can be introduced on every component of the state vector. As a result, the transition probability is the following:

$$f(\boldsymbol{x}_k|\boldsymbol{x}_{k-1}) = \mathcal{G}(\boldsymbol{x}_t - F\boldsymbol{x}_{t-1}, Q)\mathbf{1}_{[\mathbf{b};\mathbf{c}]}(\boldsymbol{x}_t) \quad (9)$$

where $\mathcal{G}(\mu, Q)$ is the multidimensional normalized centred Gaussian function, of covariance matrix Q, evaluated

at μ; $\mathbf{1}$ is a rectangular function, $\mathbf{b}$ and $\mathbf{c} \in \mathbb{R}^6$ are the lower and upper boundaries of the state vector. The domain defined by these bounds will be referred as the configuration space and denoted $\mathcal{C}$ in the following. These vectors are given by biomechanical constraints of the human body and natural range of motion.

D. STATISTICAL OBSERVATION MODEL

The proposed estimation method is based on accelerometers as they are low power and inexpensive, compared to gyroscopes. They measure linear acceleration relative to their local coordinate system, i.e. $h^{(1)}(\boldsymbol{x}_t^{(1)}, \ell_1)$ on the first link and $h^{(2)}(\boldsymbol{x}_t, L, \ell_2)$ on the second link. Any observation from an accelerometer is disturbed by noise, and taking into account this observation noise improves the estimation quality. To do so, the measurements on the ith 2D accelerometer on the second link are modelled by a statistical observation model:

$$z_t^{acc,i} = h^{(2)}(\boldsymbol{x}_t, L, \ell_i) + \boldsymbol{n}_t \quad \text{with } \boldsymbol{n}_t \sim \mathcal{N}(\mathbf{0}, R^{acc,i}) \tag{10}$$

where $R^{acc,i} \in \mathbb{R}^{2\times 2}$ is the observation noise covariance matrix.

For the purpose of comparison, measurements from a 1D gyroscope on the second segment are also modelled, as the direct observation of the total angular velocity, with a perturbation:

$$z_t^{gyr,2} = \omega_{1,t} + \omega_{2,t} + n_t^{gyr} \quad \text{with } n_t^{gyr} \sim \mathcal{N}(0, r^{gyr}) \tag{11}$$

where n_t^{gyr} is a centred Gaussian noise, of variance $r^{gyr} \in \mathbb{R}$.

For sake of simplicity, the concatenation at time t of measurements of two 2D accelerometers, or different configurations including gyroscopes detailed in section IV-A, is written as $\boldsymbol{z}_t$. Similarly, the result of the observation function providing the concatenated vector, given the appropriate parameters, is written as $h(\boldsymbol{x})$. As a result, the likelihood is expressed as:

$$p(\boldsymbol{z}_t|\boldsymbol{x}_t) = \mathcal{G}\left(\boldsymbol{z}_t - h(\boldsymbol{x}_t), R\right) \tag{12}$$

where R is the global observation noise covariance matrix. Note that we consider the measurements from different accelerometers (and gyroscope) independent, so R is diagonal and the likelihood of the observation vector gathering all sensors is proportional to the product of all individual likelihoods.

III. RECONSTRUCTION METHODS

In this section, we present the instrumental and algorithmic constraints due to the residential context that may differ from laboratory constraints. Then, we review the existing methods to estimate the kinematics of human limbs from inertial sensors. In particular, we focus on statistical methods and methods able to tackle the inverse problem. Finally, we propose a method to estimate the angular kinematics with two accelerometers on the second segment only, using a regularised particle filter.

A. CONSTRAINTS FOR RESIDENTIAL MONITORING

In the context of residential monitoring, this study aims at providing information about activities of daily living to people in their own house. It involves estimating the body motion from wearable sensors, to propose a activity classification. So the constraints on the sensors and on the estimation algorithm are different in a residential context, than for the common laboratory experiments. The constraints are the following:

1) *Battery Life:* The sensor battery should last several weeks to avoid frequent charges. This is crucial to assure that the person wears the sensor in the long-term. As a comparison, laboratory experiments usually last a few hours so the sensing possibilities are clearly different. As gyroscopes can consume 1000 times more current than accelerometers,[1] a residential system would definitely benefit from a system based on accelerometers only.
2) *Real Time Analysis:* To allow a quick reaction from medical staff to an emergency, sensor data must be processed with an appropriate frequency.
3) *Reliability:* To allow a sensible data fusion with other sensing modalities, estimated kinematics should be associated with a standard deviation.
4) *Wearability:* From the user's point of view, wearing one device is more likely acceptable than wearing two. On this basis, the study focusses on the estimation of the arm motion from one device, including two accelerometers, situated on the wrist.

Considering these constraints, the next section reviews the existing methods for estimating the joint kinematics.

B. EXISTING METHODS FOR ANGULAR KINEMATIC ESTIMATION

Inertial sensors are commonly used to monitor activities of daily living [1], as well as quality of gait and of posture. In particular, numerous methods focussing on joint angles have been proposed [25]. To estimate joint angles, most methods require at least one accelerometer on each segment [4], [5], [7], [18], [26]–[28], [29]. Indeed, if the segment is static, then in the planar case, the angle can easily be recovered from the gravity components measured by one 2D accelerometer, by evaluating the arctangent of the negative ratio of observations on axis y by axis x or a similar method using one axis only [6], [18]. The drawback of these methods is they assume the segment is static to simplify equations and do not recover full information in 3D. With one sensor only, the angle can also be estimated via a pseudo-inversion [27], [28]. The latter method has the advantage to be adaptable to a large number of sensors. With two 2D accelerometers, the Common Mode Rejection (CMR) method [25] evaluates the difference between components from both sensors and provides access to the angle [5], [7], square velocity and acceleration [4].

[1]The normal operating current is 1.8 μA for the ADXL362 accelerometer [23] and 3600 μA for the MPU-6050 gyroscope [24].

One can notice that most studies only focus on the angle estimation, while the velocity and acceleration can be estimated by linear approximation [28], CMR [4] and gradient descent [27].

Gyroscopes are often used together with accelerometers to estimate joint kinematics because they provide a direct measurement of the angular velocity with a very low noise level. Although methods using gyroscopes are often used for laboratory experiments, it is interesting to study them as they may be adapted for accelerometers only. As a first approach, the angle can be estimated by integration of the angular velocity but the offset and noise lead to an estimation error increasing with time. This can be improved by applying a high-pass filter before integration [6], but at the expense of phase lag. Then, the information from accelerometers and gyroscopes can be merged through deterministic methods such as the weighted average of the angles derived from each sensor [8], [13]. Using a threshold on the intensity of motion, one can switch between the angle derived from the accelerometer for low motion frequencies, and the angle integrated from the gyroscope for high frequencies [9], [30]. A composite filter is proposed in [17], where the angular acceleration is derived by differentiation of the gyroscope's velocity and then combined to measurements in equation 3 to extract the angle. This method has the advantage to provide the three kinematic variables without assumption of immobility and to use all data at the same time. At least, it is also possible to consider the velocity and acceleration as the derivatives of the angle, and to solve the differential equation system [31].

All methods mentioned previously are deterministic. As the observation model is nonlinear, the estimation of angular kinematics is a non-convex optimization problem. As a consequence, all these methods will provide different results as a function of the noise realisation. Moreover, their estimation is only based on observations and do not include additional information, a concept essential for this research. According to Bayes theorem, observations and prior information can be combined in the posterior distribution of the state. So the following paragraph outlines stochastic approaches based on statistical models of the state and the observation. A very popular method is the Extended Kalman Filter (EKF) which is a generalization of the Kalman Filter for nonlinear systems. The Kalman Filter is designed for linear transition and observation models. It assumes that the prior, likelihood and posterior densities are Gaussian distributions. The Kalman Filter provides, in one step, the mean which is the state estimate and the covariance matrix of the posterior density. As a consequence, it is often considered as the simplest Bayesian method. The EKF linearises the transition and observation models using the Jacobian matrices of these functions. It was applied to angle estimation using IMU inertial measurements [29] or a formulation based on quaternions [32]. This method has the advantage to provide standard deviations via the covariance matrix. The Unscented Kalman Filter (UKF) [33] extends the EKF for non Gaussian densities and estimates the posterior density using sigma points, similarly to particle filters. This method is used to estimate arm and forearm angles from an accelerometer and a gyroscope in [16].

Up to this point, existing methods require at least one set of sensors per segment which is quite feasible for a laboratory experiment, but not ideal in the long-term in a house. Applied with sensors on the end-of-line segment, they can only provide the kinematics of a single segment, or several configurations of two segments, without distinction.

Only a few studies address the inverse problem of the estimation of angular kinematics from end-of-line sensors. Reference [22] shows the angles of a 3-segment chain can be recovered from motion capture sensors on the first and second segment. In this study, the joint angles formulated by quaternions are estimated by a generalized EKF which is completed by a Gauss-Newton optimisation step. The resulting estimator is the maximum a posteriori and is associated with a covariance matrix. Its aim is very similar to ours, but the nature of sensors is quite different because they provide positions and orientations. A recent study [10] estimates the kinematics of legs during a planar squat using a single IMU in the lower back. This promising method, using a Jacobian pseudoinverse matrix, estimates three angles from a 2D accelerometer and gyroscope data filtered by a Weighted Fourier linear combiner. In particular, it tackles the inverse problem with limitations of the joint angles to avoid unrealistic estimations. This method has the asset to provide the leg angle with good accuracy. However, it presupposes a gyroscope and could not be adapted to use accelerometers only. It also does not provide standard deviations which are necessary for information fusion with other sensors.

C. PROPOSED RECONSTRUCTION METHOD

1) SECOND-SEGMENT ACCELEROMETERS

We propose to process an indirect estimation of the angular kinematics of both links, using two accelerometers located on the second link. While the estimation from second-segment sensors has already been studied [10], [22], we present an estimation method which is reasonably applicable to long-term residential monitoring. Our method, denoted I2A (for Inverse problem with 2 Accelerometers), estimates simultaneously all the components of the variable $\boldsymbol{x}_k$ from the measurements $z_k^{acc,2}(\boldsymbol{x}, L, \ell)$ of two accelerometers located at $\ell = \ell_{21}$ and $\ell = \ell_{22}$ from the joint.

2) PARTICLE FILTERING

According to Bayes theorem, information from observation and prior or transition can be combined in the posterior density. In a sequential context, it could be stated as [34]:

$$p(\boldsymbol{x}_{0:t}|z_{0:t}) = \frac{p(z_t|\boldsymbol{x}_t)f(\boldsymbol{x}_{0:t}|\boldsymbol{x}_{0:t-1})}{p(z_t|z_{0:t-1})}p(\boldsymbol{x}_{0:t-1}|z_{0:t-1}) \quad (13)$$

where $\boldsymbol{x}_{0:t}$ gathers the state vector values from time 0 to time t, and the observation values for $z_{0:t}$. One estimator of the state is the posterior mean of the filtering distribution on

the domain of the state vector ($]-\pi;\pi]$ for the angles, $\mathbb{R}$ for the other components) which is defined as following:

$$\widehat{\boldsymbol{x}_t} = \int \boldsymbol{x}_t p(\boldsymbol{x}_t|z_{0:t})d\boldsymbol{x}_t \tag{14}$$

If the system were linear and Gaussian, the state vector could be obtained by the Kalman filter. As the system is nonlinear, this integral cannot be analytically evaluated. It could be approximated using a Monte Carlo method, which means generating random samples from the posterior distribution and then computing their sum. Unfortunately, the posterior distribution is complex and difficult to sample directly.

The adopted solution is to approximate the posterior distribution by particle filtering. For extensive reviews, one can refer to [34] and [35]. The principle is to generate samples, called particles, from an importance function $q_t(\boldsymbol{x}_t|\boldsymbol{x}_{t-1}, z_t)$ and to associate each particle with a weight that enables correction of the dissimilarities between the importance and the posterior density:

$$\widehat{\boldsymbol{x}_t} = \sum_i^N w_t^{(i)} \boldsymbol{x}_t^{(i)} \tag{15}$$

where $w_t^{(i)}$ is the normalized weight of the ith particle at time t and N the number of particles. The unnormalized weight $\tilde{w}_t^{(i)}$ is defined as the ratio of the posterior probability by the importance probability. Assuming the process is Markovian, the weight can be written as the product of the weight at time $t-1$ by the incremental weight, which allows an iterative structure:

$$\begin{aligned}\tilde{w}_t^{(i)} &= \frac{p(\boldsymbol{x}_{0:t}^{(i)}|z_{0:t})}{q(\boldsymbol{x}_{0:t}^{(i)}|z_{0:t})} \\ &= \tilde{w}_{t-1}^{(i)} \frac{p(z_t|\boldsymbol{x}_t^{(i)}) f(\boldsymbol{x}_t^{(i)}|\boldsymbol{x}_{t-1}^{(i)})}{q_t(\boldsymbol{x}_t^{(i)}|\boldsymbol{x}_{t-1}^{(i)}, z_t)}\end{aligned} \tag{16}$$

Similarly, the covariance matrix $P_t \in \mathbb{R}^{6\times 6}$ can be estimated using the posterior mean, the particles and their normalized weights:

$$\widehat{P_t} = \sum_i^N w_t^{(i)} (\boldsymbol{x}_t^{(i)} - \widehat{\boldsymbol{x}_t})(\boldsymbol{x}_t^{(i)} - \widehat{\boldsymbol{x}_t})^T \tag{17}$$

Particle filtering has the advantage to estimate the posterior distribution via particles and associated weights, instead of estimating only the state vector. Unlike the EKF, the particle filter does not assume the posterior distribution is normal. It is particularly appropriate to solve this ill-posed inverse problem.

3) REGULARIZED RESAMPLING

If the importance function is significantly different from the posterior density, then most weights are very low, leaving a very small number of particles with a significant weight. This degeneracy of particles leads to a poor estimation result. To limit this phenomenon, one can resample [36] following the probability given by the weights, in order to remove useless particles and to duplicate particles with significant weights. This step of the Sequential Importance Resampling (SIR) is usually employed when the Effective Sample Size (ESS) [37] is below a given threshold.

In this study, the resampling step regularizes the posterior distribution. This post-regularized particle filter [38] smooths the estimated posterior density by adding Gaussian noise to the particles. This is equivalent to convolving the estimated posterior by a Gaussian kernel. This regularization limits the degeneracy phenomenon due to the limited number of particles and to the choice of the importance function.

4) IMPORTANCE FUNCTION

The choice of the importance function is a key element of the good operating of a particle filter. The optimal importance function is the posterior density itself but it is impossible to use in practice. The simplest choice is the transition function. In this case, the SIR method is called Bootstrap [36] and the incremental weight comes down to the likelihood. To improve the efficiency of sampling, the importance distribution should take into account the current observation. In this study, particles are generated by a Gaussian importance function $q(\boldsymbol{x}|\boldsymbol{x}_{t-1}, z_t) \sim \mathcal{N}(\mu_t^{(i)}, \Sigma_t^{(i)})$, of which mean $\mu_t^{(i)} \in \mathbb{R}^6$ and covariance matrix $\Sigma_t^{(i)} \in \mathbb{R}^{6\times 6}$ are obtained by local linearisation of the observation function h [39]. The estimation of the mean and covariance matrix is similar to the EKF.

Let's denote $\hat{H}_t$ the Jacobian matrix of the observation function h evaluated for the prediction $F\boldsymbol{x}_{t-1}^{(i)}$ of the ith particle. Then, for each particle $i = 1 \cdots N$, the inverse of the covariance matrix and the mean are given by the following expressions:

$$\left(\Sigma_t^{(i)}\right)^{-1} = Q^{-1} + \hat{H}_t^T R^{-1} \hat{H}_t \tag{18}$$

$$\begin{aligned}\mu_t^{(i)} = \Sigma_t^{(i)} \Big(& Q^{-1} F \boldsymbol{x}_{t-1}^{(i)} \\ & + \hat{H}_t^T R^{-1} (z_t - h(F\boldsymbol{x}_{t-1}^{(i)}) + \hat{H}_t F \boldsymbol{x}_{t-1}^{(i)}) \Big)\end{aligned} \tag{19}$$

Note the mean and the covariance matrix vary according to particle and time; so using this adapted importance function is computationally more expensive than using a constant density.

5) CONSTRAINED IMPORTANCE FUNCTION

The particles generated from the Gaussian importance function belongs to $\mathbb{R}$. In order to respect the limits of the configuration space $\mathcal{C}$, the mean $\mu_t^{(i)}$ of every particles are projected into $\mathcal{C}$. Thus, the importance function is based on a constrained EKF (C-EKF) with a posterior projection [40]. So, if the state variable was 1D, at least half particles statistically would belong to $\mathcal{C}$; the others would have a null weight. This projection guarantees that the posterior estimate

lies in the configuration space $\mathcal{C}$. To improve this importance function, reference [41] presents an acceptance or rejection step to ensure all particles are inside $\mathcal{C}$. However, this solution is time-consuming which is a drawback for real-time monitoring.

TABLE 1. Estimation algorithm of the state vector x_t and covariance matrix P_t by Extended Regularized Particle Filtering (ERPF).

Initialization:
$\forall i \in [\![1:N]\!]$

- Sample $\boldsymbol{x}_0^{(i)} \sim q_0(\boldsymbol{x}_0|\boldsymbol{z}_0)$,
- Associate initial importance weights $\tilde{w}_0^{(i)} = \frac{p(\boldsymbol{x}_0^{(i)}|\boldsymbol{z}_0)}{q_0(\boldsymbol{x}_0^{(i)}|\boldsymbol{z}_0)}$

Normalize weights $\left\{\tilde{w}_0^{(i)}\right\}_{i=1\cdots N}$.

Iterative step at time t:

1) Importance distribution moments: $\forall i \in [\![1:N]\!]$
   - Estimate covariance matrix $\Sigma_t^{(i)}$ by Equation 18
   - Estimate mean $\mu_t^{(i)}$ by Equation 19
   - Project $\mu_t^{(i)}$ into $\mathcal{C}$
2) Propagation: $\forall i \in [\![1:N]\!]$
   - Generate particles $\boldsymbol{x}_t^{(i)} \sim q_t(\boldsymbol{x}_t^{(i)}|\boldsymbol{x}_{t-1}^{(i)}, \boldsymbol{z}_t) = \mathcal{N}(\mu_t^{(i)}, \Sigma_t^{(i)})$
   - Update weights $\tilde{w}_t^{(i)}$ by Equation 16.
3) Normalize weights $\left\{\tilde{w}_t^{(i)}\right\}_{i=1\cdots N}$
4) If ESS $<$ threshold then regularized resampling cf. III-C3
5) Estimate state vector $\boldsymbol{x}_t$ by Equation 15
6) Estimate covariance matrix P_t by Equation 17

The resulting estimation algorithm, of which structure is presented by section III-C2, and using the regularized resampling mentioned in III-C3, is detailed by the Table 1. In the following sections, the proposed estimation method is referred as C-ERPF, for constrained Extended Regularized Particle Filter, with the I2A configuration, for Indirect estimation using 2 Accelerometers.

IV. SIMULATION OF A 2-LINK CHAIN

In this section, several sensor configurations and several estimation methods are compared, using a simulated dataset of accelerometer and gyroscope measurements.

A. SENSOR CONFIGURATIONS

As explained in section III-B, most studies focussing on joint angles use one set of sensors per segment. The simplest method is to estimate directly each angle using one 2D accelerometer per segment (DA), usually by comparison to the gravity vector. Then, one can estimate the angles from two 2D accelerometers per segment (D2A), often by CMR. To improve user acceptance, the angles and the kinematics can be estimated indirectly from sensors on the second segment only, either with two accelerometers (I2A) or one accelerometer and one gyroscope (IAG). These four configurations are represented by Fig. 3.

Table 2 compares the total operating current necessary for each configuration and their wearability. A measuring device, as an IMU, can contain several sensors, i.e. two distal

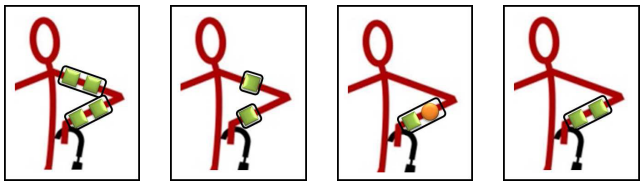

(a) D2A (b) DA (c) IAG (d) I2A

FIGURE 3. Sensor configurations to estimate angular joint kinematics. Green squares: 2D accelerometer; Orange round: 2D gyroscope. Box: link system. Outline adapted from The Saint, L. Charteris.

TABLE 2. Sensor configurations, corresponding operating current. L: length of the first segment; ℓ_{11} and ℓ_{12} (resp. ℓ_{21} and ℓ_{22}): distances of both accelerometers on the 1st link (resp. 2nd link) from the link origin. Total operating current based on ADXL362 accelerometer [23] and MPU6050 gyroscope [24].

Available data		D2A	DA	IAG	I2A
$\boldsymbol{z}_k^{acc,11}(\boldsymbol{x}_k^{(1)}, \ell_{11})$	(10)	x			
$\boldsymbol{z}_k^{acc,12}(\boldsymbol{x}_k^{(1)}, \ell_{12})$	(10)	x	x		
$\boldsymbol{z}_k^{acc,21}(\boldsymbol{x}_k^{(1\&2)}, L, \ell_{21})$	(10)	x			x
$\boldsymbol{z}_k^{acc,22}(\boldsymbol{x}_k^{(1\&2)}, L, \ell_{22})$	(10)	x	x	x	x
$z_k^{gyr,2}(\boldsymbol{x}_k^{(1\&2)})$	(11)			x	
Total operating current [μA]		8	4	3602	4
Number of link systems		2	2	1	1

accelerometers (D2A / I2A) or one accelerometer and one gyroscope (IAG). So the wearability of the configuration can evaluated by the number of apparent devices. According to Table 2, the configuration I2A is the best among the proposed configurations, in terms of power savings and wearability. Indeed, IAG is the most expensive configuration because of the gyroscope; the other three have far smaller current consumption, but I2A and DA consume half the current of D2A. Moreover, I2A and IAG are more likely to be worn by the user because they do not imply sensors on the first segment. So, our study suggests the I2A configuration for residential monitoring.

In order to assess the performances of the proposed estimation method of section III-C, simulations of realistic data are generated, according to the model presented in II. Parameters for the simulation are given in Table 3. Angles were simulated to correspond to the motion of a human arm in the sagittal plane. The sampling frequency was chosen in order to cover the range of human body motion frequencies defined as [0.1; 15] Hz by [17] for stationary states and tremors. Moreover, it is identical to the sampling frequency used in the experimentation in V-A. Then, velocities and accelerations are computed by numerical differentiation, followed by a low-pass filter. From there on, measurements are simulated from two accelerometers located on each arm segment and one gyroscope on the second segment, so as to cover all configurations previously presented. As modelled in section II-D, measurements are distorted by a Gaussian noise. Noise levels were measured on accelerometers ADXL362 and gyroscopes MPU-6050. The accelerometer simulations are shown in Fig. 4.

TABLE 3. Simulation: configuration parameters.

Configuration	Data features
$\ell_{11} = 0.10$m	$\frac{1}{\Delta T} = 50$Hz
$\ell_{12} = 0.25$m	Duration= 50s
$L = 0.30$m	$R^{acc} = 0.0036\ I_2\ (\mathrm{m/s^2})^2$
$\ell_{21} = 0.10$m	$r^{gyr} = 2.2 \times 10^{-5}\ (\mathrm{rad/s})^2$
$\ell_{22} = 0.25$m	

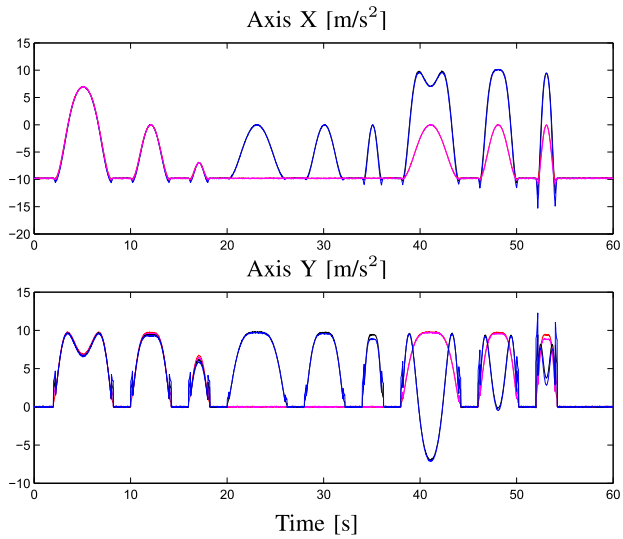

FIGURE 4. Simulations of 4 2D accelerometer measurements on a 2 link pendulum. Ordered by distance from the shoulder: red, magenta, black, blue.

B. COMPARISON OF SEVERAL ESTIMATION METHODS

The proposed method C-ERPF must be compared to some existing methods to asses its value. As explained in section III-B, the EKF is a very common method to estimate angular kinematics. In order to tackle the inverse problem we're studying, the EKF can be completed with constraints on the state vector. For instance, according to [40], the state vector of the prediction step can be projected in the interval [**b**; **c**], which is referred as prior estimate projection. This way to apply constraints is consistent with the transition statistical model of (9). This estimation is named constrained-EKF (C-EKF) in the following. The last method to be considered is the ERPF without constraint, which is equivalent to set constraints to $\pm\infty$. This comparison will allow to evaluate the usefulness of the constraints in this ill-posed problem.

C. ESTIMATION RESULTS FROM MOVEMENT SIMULATIONS

In order to evaluate the challenge that represents the proposed configuration I2A, the proposed estimation method C-ERPF (cf.III-C) is applied to the simulated dataset with the four sensor configurations. The diagonal transition covariance matrix is $Q = \mathrm{diag}([(10^{-2}\mathrm{rad})^2, (10^{-1}\mathrm{rad/s})^2, (5\ \mathrm{rad/s^2})^2])$; the lower boundary of the transition density is $\mathbf{b} = \left[-\frac{\pi}{6}, -10, -40, 0, -10, -100\right]$ and the upper boundary is $\mathbf{c} = [\pi, 10, 70, \pi, 10, 100]$ where the unit is radians for the angles, rad/s for the velocities and rad/s^2 for the accelerations. The prior density was a Gaussian distribution, of mean the true state value at time 0 and covariance matrix Q. The importance function $q_0(\boldsymbol{x}_0|z_0)$ at time 0 is the prior density. The C-ERPF was processed with $P = 3000$ particles.

TABLE 4. Simulations: Normalised estimation performances of the four sensor configurations, with the Constrained-ERPF method. Performances: norm 1 of the error between the estimated state vector and its true value, normalised by the range, averaged over time, averaged for 10 runs.

Config.	ϕ_1	ω_1	α_1	ϕ_2	ω_2	α_2
D2A	0.0087	0.0084	0.0171	0.0095	0.0190	0.0405
DA	0.0173	0.0067	0.0171	0.0233	0.0410	0.0808
IAG	0.1530	0.1308	0.1059	0.1573	0.1309	0.1384
I2A	0.1495	0.1488	0.1317	0.1499	0.1508	0.1285

Table 4 presents the estimation performances of the four sensor configurations. Note the estimation is processed 10 times for each configuration, so that the performances are averaged. Based on the simulated dataset, the best results are obtained with the D2A configuration, which provides the largest number of sensors. These estimated results are very accurate with less than 2% error on the first link kinematic variables, and 4% for the second link. In particular, both angles are estimated with less than 1% error. These results validate the proposed C-ERPF method for a direct estimation from the simulated dataset. They also show that very goods results can be obtained when four accelerometers are available.

With the DA configuration which only benefits from one accelerometer on each segment, the results are similar on the first link, but the errors are approximately doubled on the second link. So, it can be noted that a small error on the first link has repercussions on the second link.

Both remaining configurations I2A and IAG only provide measurements from the second link. As a consequence, the performances are reduced. For instance, the estimation error on the angle increases from 2% with DA to 15% in average with I2A and IAG. However, these performances are reasonably good and the estimated kinematics could be used as features for activity recognition. Overall, the errors with I2A and IAG are quite similar. The estimated velocities are slightly better with IAG because the gyroscope provides a direct measurement of the velocity with a low noise level. The estimated angles are slightly more accurate with I2A than IAG because two accelerometers are available instead of one.

This comparison highlights the challenge to estimate angular kinematics with sensors on the second segment only. It also demonstrates that this indirect estimation is possible with the C-ERPF method.

Table 5 compares the estimation performances based on the proposed I2A configuration, with the four methods EKF, C-EKF, ERPF and C-ERPF. Fig. 5 shows the estimated angles for the two reconstruction methods ERPF and C-ERPF. The poor EKF results are due to the mono-modal posterior density assumption which is not appropriate here, as it was discussed in section II-B. By projecting the predicted state vector, the

TABLE 5. Simulations: Normalised estimation performances with the accelerometers on the second segment (I2A) for several methods.

Method	ϕ_1	ω_1	α_1	ϕ_2	ω_2	α_2
EKF	0.4459	0.2170	0.4380	0.4356	0.2095	0.4477
C-EKF	1.0573	1.3047	0.6012	0.1861	1.3818	0.6189
ERPF	0.3085	0.3022	0.4031	0.3088	0.3485	0.4077
C-ERPF	0.1495	0.1488	0.1317	0.1499	0.1508	0.1285

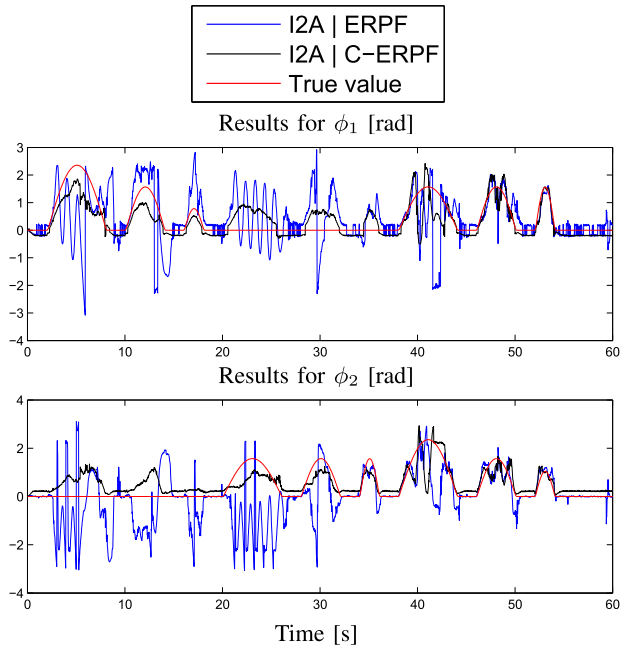

FIGURE 5. Simulations: Estimated angles with the proposed method with (C-ERPF) and without (ERPF) biomechanical constraints, with the I2A measuring configuration.

C-EKF respects the boundaries of the transition model but the resulting corrected estimate is dramatically incorrect. The ERPF error on angles is lower than EKF; however the estimated angles, as shown in Fig. 5, oscillate between positive and negative values that are similarly probable. Therefore, Fig. 5 highlights that state constraints are crucial for the reconstruction of angles in order to avoid the oscillations obtained by the ERPF method. Indeed, the angles estimated by C-ERPF are more realistic since they are inside the motion range and they have a smoother evolution. Using jointly the particle filter flexibility and state constraints, the proposed C-ERPF method provides the best results with an average error between 12% and 15% on the simulated kinematic variables.

V. EXPERIMENTS ON A HUMAN ARM

In this section, an experimental dataset collected from two subjects, using a Vicon motion capture system as reference is presented. Sensor configurations and estimation methods are compared with this dataset.

A. EXPERIMENT

The experiment consists of collecting data simultaneously from inertial sensors worn by a subject and from a reference device. This experiment was repeated on two healthy adults. The inertial sensors used were two ADXL362 3D accelerometers located on the right upper arm, two MPU-6050 sets of one 3D accelerometer and one 3D gyroscope, located on the forearm. Configurations are detailed in Table 6.

TABLE 6. Experiment: Configuration parameters.

Configuration no.1	Configuration no.2	Data features
$\ell_{11} = 0.24$m	$\ell_{11} = 0.14$m	$\frac{1}{\Delta T} = 50$Hz
$\ell_{12} = 0.27$m	$\ell_{11} = 0.17$m	$R^{acc} = 0.0036\ I_2\ (\mathrm{m/s^2})^2$
$L = 0.30$m	$L = 0.29$m	$r^{gyr} = 2.2 \times 10^{-5}\ (\mathrm{rad/s})^2$
$\ell_{21} = 0.18$m	$\ell_{21} = 0.20$m	
$\ell_{22} = 0.26$m	$\ell_{22} = 0.24$m	
Duration = 46s	Duration = 50s	

Data were collected at 50 Hz while the arm was moved approximately in the sagittal plane. The sampling frequency was chosen from a limited number of possibilities, in order to capture adequately human motions as explained in IV-A, and to offer a good compromise between accuracy and energy cost. The protocol was a sequence of three motions: moving the forearm only, moving the arm straight and reaching. Each sequence was repeated three times at different speeds that can be described as slow, intermediate and very fast.

Fig. 6 shows the accelerometer measurements from the four sensors on the arm. During the periods when the first link curves(red and magenta), which represent the upper accelerometers, are roughly stable while the second link curves (blue and black) are raising, only the forearm is moved. When all curves are approximately superposed, the arm is kept straight.

For reference, 4 motion capture markers are positioned on each segment of the shoulder, upper and forearm. The position and orientation of the markers are provided by the Vicon system using 14 cameras. Then, the motion plane is identified by Principal Component Analysis of the 3D coordinates of the markers. Finally, the angles ϕ_1 and ϕ_2 of the arm are inferred from the markers' positions projected in the motion plane and considered as the reference in the following.

TABLE 7. Experiment: Normalised estimation performances of the four sensor configurations, with the Constrained-ERPF method, averaged on datasets from both subjects.

Config.	ϕ_1	ω_1	α_1	ϕ_2	ω_2	α_2
D2A	0.1683	0.0729	0.0693	0.1481	0.1094	0.1662
DA	0.1659	0.0724	0.0621	0.1938	0.1601	0.1709
IAG	0.3184	0.1825	0.1114	0.2408	0.1915	0.1457
I2A	0.2219	0.0969	0.0668	0.1553	0.0973	0.0675

B. ESTIMATION RESULTS ON EXPERIMENT

Table 7 compares the performances of the four sensor configurations from the experimental dataset, using the C-ERPF estimation method. Such results cannot be compared to other reconstruction methods using gyroscopes [10] or motion capture systems [22] because the nature of sensors and thus the amount of available information are different. Similarly to the

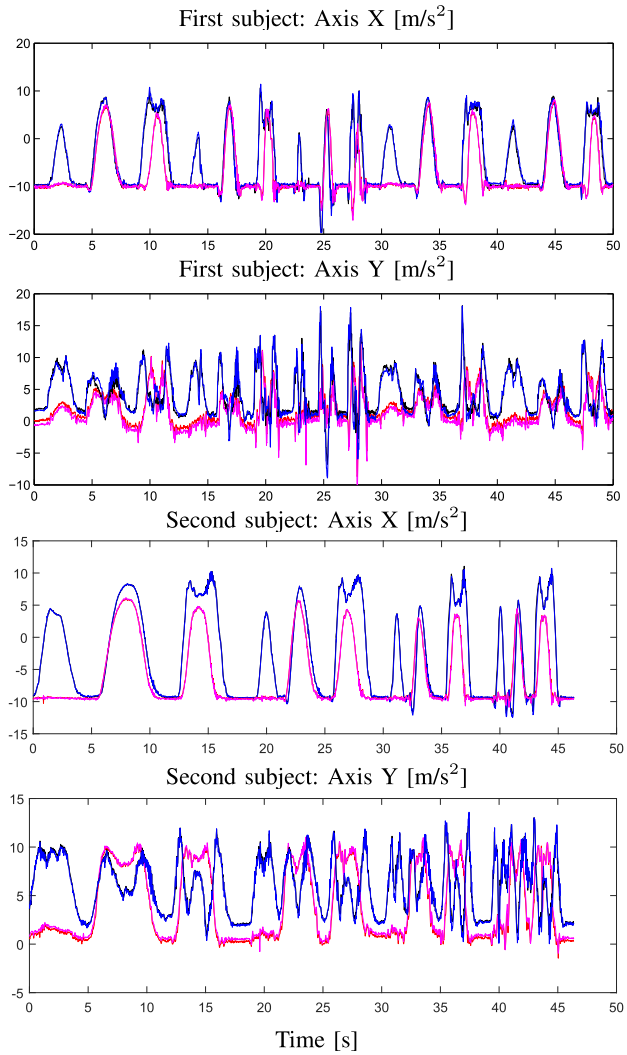

FIGURE 6. Accelerometer measurements on the arm of both subjects. Sensors on first link at ℓ_{11} (red) and ℓ_{12} (magenta) and on second link at ℓ_{21} (black) and ℓ_{22} (blue).

simulation-based results, the best performances are achieved with the D2A and DA configurations which contain one or two accelerometers on each segment. The performances with the I2A configuration are promising, with an average error of 7% on the accelerations, 10% on the velocities and 15% on the second angle. The augmentation of the errors compared to simulation performances in Table 4 is due to several factors. The major one is the approximation of the motion in a plane; the projection of Vicon positions in the motion plane distorts the reference angles. A 3D model of the arm should reduce this problem. Then, the calibration of the orientation of the inertial sensors and the Vicon sensors is another source of error. Finally, the global motion of the arm is perturbed locally by the motion of the sensors on the skin.

In Table 8, the performances of four estimation methods are compared, based on the proposed I2A configuration. The EKF and C-EKF provide poor results, notably for the angles with an average of 26% and 30%. It is due to the fact that EKF methods assume the posterior distribution is Gaussian,

TABLE 8. Experiment: Normalised estimation performances with the accelerometers on the second segment (I2A) for several methods, averaged on datasets from both subjects.

Method	ϕ_1	ω_1	α_1	ϕ_2	ω_2	α_2
EKF	0.2647	0.0982	0.0830	0.2551	0.1224	0.0831
C-EKF	0.2629	0.1405	0.1103	0.3380	0.1545	0.1026
ERPF	0.2961	0.0814	0.0613	0.1529	0.0823	0.0663
C-ERPF	0.2219	0.0969	0.0668	0.1553	0.0973	0.0675

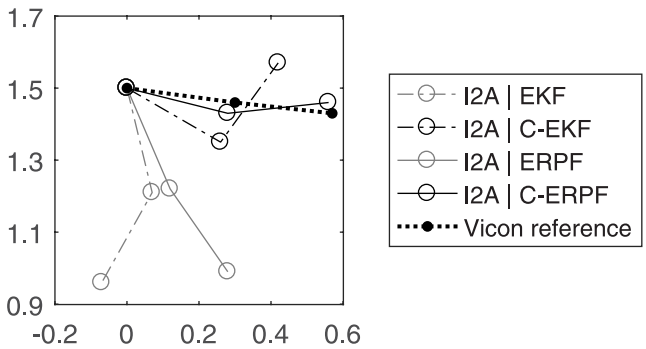

FIGURE 7. Experiment: Estimated configuration of the arm of the first subject at time $t = 8.8$s, with different methods. Position of arm segments [m].

therefore mono-modal. According to Fig. 1 which represents the arm configuration estimated with the four methods at a given time, the EKF results is clearly not possible because of the elbow constraint. The C-EKF result which is the positive symmetric of the EKF is more realistic but ϕ_2 is overestimated. So adding constraints to the EKF can improve the estimation of angles but is not sufficient to get meaningful results. The results of the ERPF are slightly better than EKF and C-EKF, with 8% or less of error on velocities and accelerations and 15% on the second angle. These performances are consistent with Fig. 8 where ϕ_2 is well estimated by ERPF and C-ERPF. For instance at time $t = 8.8$s in Fig. 7, ϕ_1 is underestimated but ϕ_2 is very close to the true value. This highlights the asset of the particle filter which allows more flexibility for the posterior distribution. However, the ERPF estimation error of the first angle (30%) is twice as high as on the second angle (15%). Indeed, the second segment is equipped with two accelerometers, whereas the first angle is only unmixed from the second angle. The ERPF angle ϕ_1 oscillates between positive and negative values that must be equally probable. In contrast, the C-ERPF angle ϕ_1 only takes values above $\pi/6$ and is closer to the reference value and more smooth. Thanks to the use of constraints, the C-ERPF method estimates angles with a better accuracy (22% on the first, 15% on the second) and similar performances as EPRF for velocities and accelerations.

C. DISCUSSION

The experiment used in this section was collected during a relatively short duration. It is well known that long-term monitoring can lead to drift in the estimation of orientation and position. Reference [29] shows that estimating orientation using a Kalman Filter reduces the drift. Therefore, the

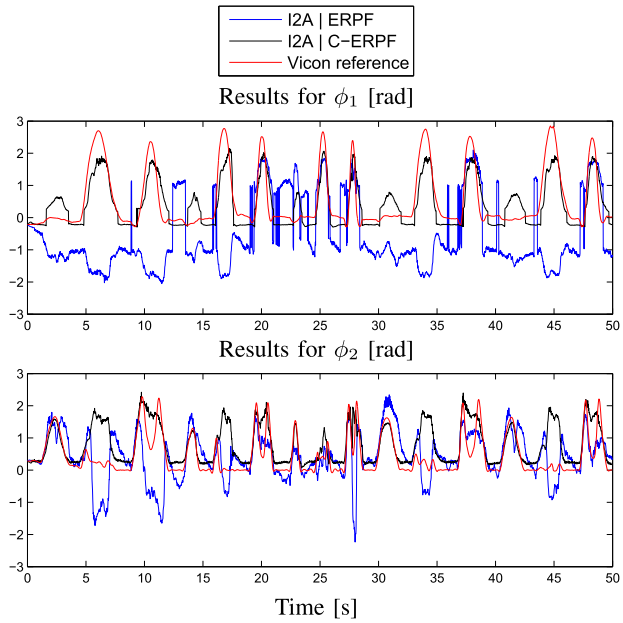

FIGURE 8. Experiment: Estimated angles of the first subject's arm, with the proposed method with (C-ERPF) and without (ERPF) biomechanical constraints, with the I2A measuring configuration.

C-ERPF method based on an EKF importance function will limit the estimation drift.

The main difficulty of our problem is that it is an ill-posed inverse problem which means several solutions (arm configurations) are possible given some observations. Only a few data are available because some sensors are missing on the upper arm. To select a realistic arm configuration, strong prior information needs to be added to the problem, and this information is contained in the kinematic model (II.A), the transition model (II.C) and the observation model (II.D). In particular, we need to define some biomechanical constraints in the transition distribution, which describe the typical limits of subjects. To accept the possibility of an inverted elbow, we can extend the lower constraint of the angle ϕ_2 to negative values such as -15 degrees. However, the limitation of our work is that we cannot reconstruct realistic arm configurations most of the time and rare configurations sometimes. Extending the biomechanical limits for a few cases would deteriorate the reconstruction accuracy for a majority of typical cases. This limitation does not impact the validity of our method which aims at reconstructing the general tendency of kinematics from a small amount of data. An inverted elbow would be reconstructed as a straight arm; for instance, such approximation would be acceptable for activity monitoring. Our strategy is sensitive to the sensor placement via the variables ℓ_i of the sensor distance from the joint and to the sensor alignment as we use a 2D kinematic model. This reconstruction method is a part of a whole processing stream. For instance, a pre-processing stage can filter collected inertial data to reduce noise. In this stage, signals can be re-aligned using a pre-calibration, or an iterative calibration running during a stationary phase. Then, the reconstruction stage applies to the corrected signals and provides kinematics. Finally, a higher-level processing stage can extract statistical features of kinematics and allows activity classification for instance. Concerning the sensor misplacement along segments, the variable ℓ_i which is a linear dependency of the system can be estimated as an additional variable during a first stage.

VI. CONCLUSION

A novel approach to the reconstruction of human movement from incomplete data has been outlined for a 2 dimensional arm kinematic model. The benefit of this approach is that the reconstruction can use additional information, should it be available, to reduce errors. The principal focus of this research is to assess health benefits of long term monitoring in a residential environment although the concept will extend to other areas of human movement measurement and assessment. The proposed strategy is based on measurements from two accelerometers only on the forearm, which makes it an ill-posed problem. The dual accelerometer has benefits in terms of a lower energy consumption when compared to gyroscopes. The reconstruction method is a post-regularized particle filter (C-ERPF), with an importance function whose moments are computed via an constrained EKF linearisation. Several sensor configurations were compared in terms of estimation performances, as well as power consumption and user acceptance. A system based on two accelerometers on the second segment (called I2A) has the lowest necessary operating current and the smallest physical size. Moreover, the proposed C-ERPF was compared to other estimation methods EKF, Constrained-EKF and ERPF. The comparison highlights the relevance of the particle filter compared to EKF methods, as the posterior distribution is estimated without shape assumption. The boundaries of the transition model are also a key point of the reconstruction process in order to respect the elbow angular constraint and to avoid unrealistic estimates. So the proposed C-ERPF method coupled with the I2A configuration provide promising results with 19% error on average in both angles, compared to the motion capture reference, 10% on velocities and 7% on accelerations. These performances are in relation with the amount of information available both from sensors and transition densities. Indeed, there is no sensor on the upper arm of which the angle ϕ_1 is reconstructed and the constraints on the configuration space are relatively weak. Thus this paper shows the practicability of kinematics reconstruction from a small number of accelerometers worn on specific points on the body such as the forearm and wrist.

ACKNOWLEDGMENT

The authors would like to thank Christophe Andrieu from the University of Bristol for advising on particle filters. They would like to thank Peter Scarfe and Rachel King from the University of Reading, and Malcolm Burnett from the University of Southampton, for their help with the motion capture data collections. E. Villeneuve was with the University of Reading, U.K.

REFERENCES

[1] A. Godfrey, R. Conway, D. Meagher, and G. ÓLaighin, "Direct measurement of human movement by accelerometry," *Med. Eng. Phys.*, vol. 30, no. 10, pp. 1364–1386, Dec. 2008.

[2] C. Chen, R. Jafari, and N. Kehtarnavaz, "Improving human action recognition using fusion of depth camera and inertial sensors," *IEEE Trans. Human-Mach. Syst.*, vol. 45, no. 1, pp. 51–61, Feb. 2015.

[3] A. Pantelopoulos and N. G. Bourbakis, "A survey on wearable sensor-based systems for health monitoring and prognosis," *IEEE Trans. Syst., Man, Cybern. C, Appl. Rev.*, vol. 40, no. 1, pp. 1–12, Jan. 2010.

[4] K. Liu, T. Liu, K. Shibata, Y. Inoue, and R. Zheng, "Novel approach to ambulatory assessment of human segmental orientation on a wearable sensor system," *J. Biomech.*, vol. 42, no. 16, pp. 2747–2752, Dec. 2009.

[5] A. T. M. Willemsen, C. Frigo, and H. B. K. Boom, "Lower extremity angle measurement with accelerometers-error and sensitivity analysis," *IEEE Trans. Biomed. Eng.*, vol. 38, no. 12, pp. 1186–1193, Dec. 1991.

[6] R. Takeda, S. Tadano, M. Todoh, M. Morikawa, M. Nakayasu, and S. Yoshinari, "Gait analysis using gravitational acceleration measured by wearable sensors," *J. Biomech.*, vol. 42, no. 3, pp. 223–233, Feb. 2009.

[7] M. D. Djurić-Jovičić, N. S. Jovičić, and D. B. Popović, "Kinematics of gait: New method for angle estimation based on accelerometers," *Sensors*, vol. 11, no. 11, pp. 10571–10585, Jan. 2011.

[8] T. Seel, J. Raisch, and T. Schauer, "IMU-based joint angle measurement for gait analysis," *Sensors*, vol. 14, no. 4, pp. 6891–6909, Jan. 2014.

[9] F. Alonge, E. Cucco, F. D'Ippolito, and A. Pulizzotto, "The use of accelerometers and gyroscopes to estimate hip and knee angles on gait analysis," *Sensors*, vol. 14, no. 5, pp. 8430–8446, Jan. 2014.

[10] V. Bonnet, C. Mazzà, P. Fraisse, and A. Cappozzo, "Real-time estimate of body kinematics during a planar squat task using a single inertial measurement unit," *IEEE Trans. Biomed. Eng.*, vol. 60, no. 7, pp. 1920–1926, Jul. 2013.

[11] J. Favre, B. M. Jolles, R. Aissaoui, and K. Aminian, "Ambulatory measurement of 3D knee joint angle," *J. Biomech.*, vol. 41, no. 5, pp. 1029–1035, Jan. 2008.

[12] D. J. Weber *et al.*, "BIONic WalkAide for correcting foot drop," *IEEE Trans. Neural Syst. Rehabil. Eng.*, vol. 13, no. 2, pp. 242–246, Jun. 2005.

[13] E. Chalmers, J. Le, D. Sukhdeep, J. Watt, J. Andersen, and E. Lou, "Inertial sensing algorithms for long-term foot angle monitoring for assessment of idiopathic toe-walking," *Gait Posture*, vol. 39, no. 1, pp. 485–489, Jan. 2014.

[14] W. Zeng and C. Wang, "Human gait recognition via deterministic learning," *Neural Netw.*, vol. 35, pp. 92–102, Nov. 2012.

[15] V. Lugade, E. Fortune, M. Morrow, and K. Kaufman, "Validity of using tri-axial accelerometers to measure human movement—Part I: Posture and movement detection," *Med. Eng. Phys.*, vol. 36, no. 2, pp. 169–176, Feb. 2014.

[16] M. El-Gohary and J. McNames, "Shoulder and elbow joint angle tracking with inertial sensors," *IEEE Trans. Biomed. Eng.*, vol. 59, no. 9, pp. 2635–2641, Sep. 2012.

[17] R. A. Hyde, L. P. Ketteringham, S. A. Neild, and R. J. S. Jones, "Estimation of upper-limb orientation based on accelerometer and gyroscope measurements," *IEEE Trans. Biomed. Eng.*, vol. 55, no. 2, pp. 746–754, Feb. 2008.

[18] T. Wolff, A. Lasso, M. Eblenkamp, E. Wintermantel, and G. Fichtinger, "C-arm angle measurement with accelerometer for brachytherapy: An accuracy study," *Int. J. Comput. Assist. Radiol. Surgery*, vol. 9, no. 1, pp. 137–144, Jan. 2014.

[19] N. Zhu *et al.*, "Bridging e-health and the Internet of Things: The sphere project," *IEEE Intell. Syst.*, vol. 30, no. 4, pp. 39–46, Jul./Aug. 2015.

[20] M. Ghamari, B. Janko, R. S. Sherratt, W. Harwin, R. Piechockic, and C. Soltanpur, "A survey on wireless body area networks for ehealthcare systems in residential environments," *Sensors*, vol. 16, no. 6, p. 831, 2016. [Online]. Available: http://www.mdpi.com/1424-8220/16/6/831

[21] S. Gaglio, G. L. Re, and M. Morana, "Human activity recognition process using 3-D posture data," *IEEE Trans. Human-Mach. Syst.*, vol. 45, no. 5, pp. 586–597, Oct. 2015.

[22] E. Todorov, "Probabilistic inference of multijoint movements, skeletal parameters and marker attachments from diverse motion capture data," *IEEE Trans. Biomed. Eng.*, vol. 54, no. 11, pp. 1927–1939, Nov. 2007.

[23] *Digital Output MEMS Accelerometer ADXL362*, Analog Devices, Norwood, MA, USA, 2013.

[24] *MPU-6000 and MPU-6050 Product Specification Revision 3.4*, InvenSense Inc., San Jose, CA, USA, 2013.

[25] P. Cheng and B. Oelmann, "Joint-angle measurement using accelerometers and gyroscopes—A survey," *IEEE Trans. Instrum. Meas.*, vol. 59, no. 2, pp. 404–414, Feb. 2010.

[26] J.-H. Chen, S.-C. Lee, and D. B. DeBra, "Gyroscope free strapdown inertial measurement unit by six linear accelerometers," *J. Guid., Control, Dyn.*, vol. 17, no. 2, pp. 286–290, Mar. 1994.

[27] S. O. H. Madgwick, A. J. L. Harrison, P. M. Sharkey, R. Vaidyanathan, and W. S. Harwin, "Measuring motion with kinematically redundant accelerometer arrays: Theory, simulation and implementation," *Mechatronics*, vol. 23, no. 5, pp. 518–529, 2013.

[28] A. Caroselli, F. Bagalà, and A. Cappello, "Quasi-real time estimation of angular kinematics using single-axis accelerometers," *Sensors*, vol. 13, no. 1, pp. 918–937, Jan. 2013.

[29] H. Zhou and H. Hu, "Reducing drifts in the inertial measurements of wrist and elbow positions," *IEEE Trans. Instrum. Meas.*, vol. 59, no. 3, pp. 575–585, Mar. 2010.

[30] H. Dejnabadi, B. M. Jolles, E. Casanova, P. Fua, and K. Aminian, "Estimation and visualization of sagittal kinematics of lower limbs orientation using body-fixed sensors," *IEEE Trans. Biomed. Eng.*, vol. 53, no. 7, pp. 1385–1393, Jul. 2006.

[31] D. Giansanti, G. Maccioni, and V. Macellari, "The development and test of a device for the reconstruction of 3-D position and orientation by means of a kinematic sensor assembly with rate gyroscopes and accelerometers," *IEEE Trans. Biomed. Eng.*, vol. 52, no. 7, pp. 1271–1277, Jul. 2005.

[32] A. M. Sabatini, "Quaternion-based extended Kalman filter for determining orientation by inertial and magnetic sensing," *IEEE Trans. Biomed. Eng.*, vol. 53, no. 7, pp. 1346–1356, Jul. 2006.

[33] S. J. Julier and J. K. Uhlmann, "Unscented filtering and nonlinear estimation," *Proc. IEEE*, vol. 92, no. 3, pp. 401–422, Mar. 2004.

[34] P. M. Djuric *et al.*, "Particle filtering," *IEEE Signal Process. Mag.*, vol. 20, no. 5, pp. 19–38, Sep. 2003.

[35] O. Cappe, S. J. Godsill, and E. Moulines, "An overview of existing methods and recent advances in sequential Monte Carlo," *Proc. IEEE*, vol. 95, no. 5, pp. 899–924, May 2007.

[36] N. J. Gordon, D. J. Salmond, and A. F. M. Smith, "Novel approach to nonlinear/non-Gaussian Bayesian state estimation," *IEE Proc. F-Radar Signal Process.*, vol. 140, no. 2, pp. 107–113, Apr. 1993.

[37] J. S. Liu, "Metropolized independent sampling with comparisons to rejection sampling and importance sampling," *Statist. Comput.*, vol. 6, no. 2, pp. 113–119, Jun. 1996.

[38] C. Musso, N. Oudjane, and F. Legland, "Improving regularized particle filters," in *Sequential Monte Carlo Methods in Practice*, vol. 12. New York, NY, USA, Springer-Verlag, 2001, pp. 247–271.

[39] A. Doucet, S. Godsill, and C. Andrieu, "On sequential Monte Carlo sampling methods for Bayesian filtering," *Statist. Comput.*, vol. 10, no. 3, pp. 197–208, Jul. 2000.

[40] D. Simon, "Kalman filtering with state constraints: A survey of linear and nonlinear algorithms," *IET Control Theory Appl.*, vol. 4, no. 8, pp. 1303–1318, Aug. 2010.

[41] L. Lang, W.-S. Chen, B. R. Bakshi, P. K. Goel, and S. Ungarala, "Bayesian estimation via sequential Monte Carlo sampling—Constrained dynamic systems," *Automatica*, vol. 43, no. 9, pp. 1615–1622, 2007.

EMMA VILLENEUVE received the master's degree in physics from the School of Engineering PHELMA, Grenoble, in 2009, the master's degree in signal and image processing from the Grenoble Institute of Technology, France, in 2009, and the Ph.D. degree in signal processing on estimation and deconvolution methods for astrophysical hyperspectral data from the University of Toulouse, France, in 2012. From 2013 to 2015, she was a Research Assistant with the University of Reading, U.K. She is currently an Associate Research Fellow with the NIHR CLAHRC South West Peninsula, University of Exeter, U.K. Her research interests are in the areas of statistical signal processing, with specific focus on healthcare applications.

WILLIAM HARWIN is currently a Professor of Interactive Systems with the University of Reading. His research interests include technology and healthcare, human-robot interactions, haptic interfaces, healthcare sensors in a residential environment, and the emerging field of cognitive robotics. Haptics research in includes the control, rendering, and applications, most recently activity was work with Kings College on the haptel Project that explore haptics as an educational tool in dental education. He has a long standing interest in assistive and rehabilitation robotics with a specific interest in neurorehabilitation for individuals following a stroke and is a past Chair of the IEEE ICORR conference series.

WILLIAM HOLDERBAUM received the M.Sc. degree in automatic control from the University of Reims Champagne–Ardenne, Reims, France, in 1993 and the Ph.D. degree from the University of Lille, Lille, France, in 1999. He was a Research Assistant with the University of Glasgow, Glasgow, U.K., from 1999 to 2001. He is currently a Professor with the School of Systems Engineering, University of Reading. Furthermore, he has authored papers in the area of geometric control theory in particular Hamiltonian systems and optimization problems. His research interests are in control theory and its applications, focused on rehabilitation engineering and in particular robust control for unsupported paraplegic standing, further research relates to control theory in the definition of multiple agent systems for distributed network composed of storages, loads and generators. This research uses the mathematical engineering skills in order to minimize the energy consumption.

BALAZS JANKO received the M.Eng. degree with the University of Reading in 2009, and the Ph.D. degree in 2014, with a thesis on a dual-drive robotic joint actuator design. He is currently a Research Assistant with the University of Reading. His current research interests are low-power wearable electronics, robotics, and haptics.

R. SIMON SHERRATT (M'97–SM'02–F'12) received the B.Eng. degree in electronic systems and control engineering from Sheffield City Polytechnic, U.K., in 1992, and the M.Sc. degree in data telecommunications and the Ph.D. degree in video signal processing from the University of Salford, U.K., in 1994 and 1996, respectively. In 1996, he has appointed as a Lecturer in electronic engineering with the University of Reading, where he is currently a Professor of Biosensors. His research topic is signal processing and communications in consumer electronic devices focusing on wearable devices and healthcare. He received the first place IEEE Chester Sall Memorial Award in 2006, and the second place Award in 2016. He is the Editor-in-Chief of the IEEE Transactions on Consumer Electronics and a Reviewer of the IEEE Sensors Journal on Wearable Sensors.